APEM journal

Advances in Production Engineering & Management
Volume 19 | Number 1 | March 2024 | pp 46–64
https://doi.org/10.14743/apem2024.1.492

ISSN 1854-6250
Journal home: apem-journal.org
Original scientific paper

Predicting the deep drawing process of TRIP steel grades using multilayer perceptron artificial neural networks

Sevšek, L.[a], Vilkovský, S.[b], Majerníková, J.[b], Pepelnjak, T.[a,*]

[a]Forming Laboratory, Faculty of Mechanical Engineering, University of Ljubljana, Ljubljana, Slovenia
[b]Department of Technologies, Materials and Computer Aided Production, Technical University of Košice, Košice, Slovakia

ABSTRACT

TRIP (Transformation Induced Plasticity) steels belong to the group of advanced high-strength steels. Their main advantage is their excellent strength combined with high ductility, which makes them ideal for deep drawing processes. The forming of TRIP steels in the deep drawing process enables the production of a thin-walled final product with superior mechanical properties. For this reason, this study presents comprehensive research into the deep drawing of cylindrical cups made from TRIP steel. The research focuses on three main aspects of the deep drawing process, namely the sheet metal thinning, the maximum force value and the ear height as a result of the anisotropic material behaviour. Artificial neural networks (ANNs) were built to predict all the mentioned output parameters of the part or the process itself. The ANNs were trained using data obtained from a sufficient number of simulations based on the finite element method (FEM). The ANN models were developed based on variable material properties, including anisotropic parameters, blank holding force, blank diameter, and friction coefficient. A good agreement between simulation, ANN and experimental results is evident.

ARTICLE INFO

Keywords:
Forming;
Deep drawing;
TRIP steel;
Artificial neural network (ANN);
Finite element methods (FEM);
Modelling;
Simulation

**Corresponding author:*
Tomaz.Pepelnjak@fs.uni-lj.si
(Pepelnjak, T.)

Article history:
Received 25 March 2024
Revised 24 April 2024
Accepted 26 April 2024

1. Introduction

The development of materials for vehicle production faces the challenge of solving diverse and often conflicting requirements. These include the need to reduce vehicle weight while providing high levels of weldability, formability, joinability, and sufficient stiffness or mechanical strength to increase the safety of passengers. In addition, it is important to optimize the simple installation of components, maintain surface resistance in demanding conditions, and preserve aesthetic properties. In today's automotive environment, meeting fuel efficiency and environmental standards within economic constraints is critical [1-3]. Cost reduction can be considered one of the main interests for companies in the modern era [4]. Different advanced forming methods have been developed to make custom made goods at a reasonable price [5]. Given these complex requirements, the choice of materials plays a key role in shaping the car's structure. High-strength steels (HSS) have demonstrated the ability to strike a balance between cost-effectiveness, weight consideration and favourable mechanical properties [6, 7].

Current research is focused on advanced high-strength steels (AHSS) and ultra-high-strength steels (UHSS), mainly composed of martensitic steels. The AHSS category includes two-phase steels and TRIP (Transformation Induced Plasticity) steels. These groups of materials exhibit mechanical properties that meet stringent environmental standards and customer requirements while remaining economically affordable for manufacturers [1-3].

1.1 Fundamentals of TRIP steels

TRIP steels hold significant appeal for the automotive industry in constructing the body-in-white due to their enhanced mechanical properties, formability, and exceptional energy absorption during a crash [8]. The microstructure of TRIP comprises distinct phases, including ferrite, austenite, martensite, and bainite, contributing to the high performance of the steel [9]. The TRIP effect, employed to improve formability and strength, is rooted in a lattice transformation. The face-centred cubic (fcc) austenite transforms, without diffusion, into either the body-centred cubic (bcc) martensite (α-martensite) or a hexagonal martensite phase (β-martensite). The bcc crystal phase is more stable, and the hexagonal phase transitions to bcc depending on the conditions [10, 11]. These diverse phases are not only beneficial for forming processes but also play a crucial role in the crash behaviour of components. However, as mechanical properties are directly linked to microstructural evolution, local stress and strain conditions impact both forming and failure behaviour. Therefore, understanding the interaction among microstructure, stress and strain conditions, and the occurrence of failure is essential [12].

1.2 Fundamentals of deep drawing

Deep drawing is a sheet metal forming process which are used to plastically deform the sheet metal into the desired shape of the final product [13]. The deep drawing process, widely utilized across industries, involves forming sheet metal for a variety of applications. Its uses span from crafting automotive components, products in the arms industry, and aerospace parts to forming tubes for medication and perfume, pots, pans, and various kitchen appliances. This method relies on forming production parts with either simple or intricate designs through substantial plastic deformation [14, 15]. Throughout the deep drawing process, potential defects may arise, such as surface scratches, wrinkling of walls and flanges, tearing, and earing [16, 17]. The effectiveness of the deep drawing process is heavily dependent on material properties, geometric considerations, and technological parameters. Key material factors encompass elasticity, plasticity, and anisotropy. Additionally, significant roles are played by parameters like punch velocity, blank holding pressure, and lubrication. The radius of the punch and die, blank thickness, and the clearance between the punch and die also contribute to the process. Incorrectly defining these parameters can result in common defects of the deep drawing process [18, 19].

Earing, a distinctive defect marked by the development of a wavy edge at the open end of the cup, is a notable issue in the deep drawing process. Numerous recent studies have addressed earing defects [20, 21]. Colgan and Monaghan [22] explored key parameters in the deep drawing process, including punch and die radii, punch velocity, friction, and draw depth. Using ANOVA software, they calculated the percentage contributions of each factor. Interestingly, punch velocity emerged as the fourth most crucial parameter, particularly impacting wall thickness deviation. Seth *et al.* [23] investigated the formability of steel sheets subjected to high-velocity impact from an electromagnetically launched punch at speeds of 50 and 220 m/s. Their experiments involved five different steel specimens with varying thicknesses, revealing failure strains ranging from 30 % to 50 %. Notably, the study observed that higher forming velocities correlate with increased formability. Huang *et al.* [24] examined the influence of blank thickness and fracture thickness on forming limits. Fracture strain, derived from a uniaxial tension test, served as the fracture criterion. The assumption was made that the blank fractures when its thickness reaches the fracture thickness in any section. The study involved the analysis of square cup drawing and elliptical hole flanging. Chalal *et al.* [25] determined forming limit diagrams using different localization criteria, such as the criterion based on the maximum second-time derivative of thickness strain, the criterion based on the ratio of equivalent plastic strain increment, the maximum punch force criterion, and the loss of ellipticity. ABAQUS/Explicit tool was employed for their analysis [25]. Gusel *et al.* [26]

focused on the forming of high-strength steel sheets (DP780 and DP1180HD) by deep drawing. The influence of yield stress, tensile strength, blank holder force and punch speed on the output parameter of cup height was evaluated [26]. The fracture problems during deep drawing were successfully predicted using genetic modelling.

1.3 Simulation using finite element method

Simulations allow the prediction of crucial outcomes within the system or process itself, using the computer environment. A correctly created simulation model of a forming process enables fast and reliable prediction of key output parameters. A small discrepancy between experimental and simulation results shows the general correctness of the set simulation model. Simulations were carried out as part of this study to predict three key output parameters of the deep drawing process of TRIP steel. A sufficient number of simulations with different input parameter values and corresponding output results were used as the basis for building an artificial neural network (ANN) for each target output parameter. The simulations based on the finite element method (FEM) were carried out in the ABAQUS simulation environment. The material properties, the geometric properties of the blank and the tools as well as the kinematics of the deep drawing process were simulated. FEM simulations can be carried out with different calculation methods, finite element types and in different simulation environments [27]. The FEM simulation of the deep drawing process can be very time-consuming [28]. The use of the explicit calculation method provides acceptable accuracy with faster calculation compared to the implicit method [29]. For this reason, the explicit method was chosen for all 50 simulations in the study presented here.

The study by Vrh *et al.* [30] focused on the constitutive modelling of anisotropic plates and the prediction of the earing for the round cup drawing using the FEM method. Shell finite elements with reduced integration were used in the ABAQUS/Explicit simulation environment [30]. Bandyopadhyay *et al.* [31] evaluated the limiting drawing ratio (LDR) of tailor welded blanks using a deep drawing test. FEM models of the deep drawing process considered the anisotropy of the sheets and the inhomogeneous properties in the welded zone of the tailor welded blanks [31]. The simulations were performed with the nonlinear solver Lsdyna-971 using shell elements [31] The study by Dwivedi and Agnihotri [32] focused on testing different materials for deep drawing of cylindrical cups without using a blank holder. The ANSYS 14.0 simulation environment was used to determine the limit drawing ratio [32]. Magnesium alloys develop a crystallographic texture and plastic anisotropy during rolling, resulting in ear formation during deep drawing of such sheets [33]. This was investigated in the study by Walde and Riedel [33], who performed FEM simulations of the deep drawing process in ABAQUS/Explicit environment using C3D8R solid brick elements with four elements across the sheet thickness. It was found that the earing pattern depends on the initial texture and on the development of the texture during the forming process under investigation [33].

In the study by Engler and Aretz [34], S4R shell elements with reduced integration were used in the ABAQUS simulation environment for the FEM simulation of the deep drawing process of various anisotropic aluminium alloys. In the study by Luyen *et al.* [35], FEM simulations of the deep drawing of cold-rolled carbon steel were carried out in the ABAQUS simulation environment. The simulations were used to determine the fracture heights of cylindrical cups and were validated with experimental results [35]. Another aim of the simulations and experiments in the study by Luyen *et al.* [35] was to investigate the effects of the blank holder force, the punch radius and the drawing ratio on the fracture height. Simulations and experiments showed that increasing the blank holder force reduces the fracture height and increasing the punch radius increases the fracture height [35]. Jayahari *et al.* [36] investigated the formability of austenitic stainless steel 304 at different temperatures under warm conditions during the deep drawing process of a cylindrical cup. The explicit FEM analysis was performed in the LS-DYNA program for forming at room temperature and other temperatures up to 150°C [36]. Shell elements were used for the blank and the tools, as this results in a shorter calculation time [36]. Shell finite elements were also used in the study presented here.

1.4 Fundamentals of neural networks

Artificial intelligence can contribute to sustainable manufacturing [37]. With advances in manufacturing intelligence, information technology is part of the automated production technologies that are the main contributors to industrial change today [38]. Artificial intelligence models used in the field of metal forming use process parameters as input parameters and forming results as output parameters [37]. One special branch of such models are neural network models, which are expressed by a nonlinear function of the weighted sum of inputs [37]. Artificial neural network (ANN) is a set of neurons and connections between them with adjustable weights [39]. Commonly used type of ANNs are the multi-layer neural networks, which consist of an input layer, one or more hidden layers, and an output layer [39, 40]. Neurons of each layer are connected to each other by connection links with adjustable weights [39]. These weights are adjusted during the training process of the neural network, commonly through the backpropagation algorithm, where the input-output example patterns are presented to the neural networks [39]. The main advantage of ANNs is the data-driven self-adaptive capabilities that allow ANNs to adapt to the data they have been trained on [41]. A basic structure of ANN is presented in Fig. 1.

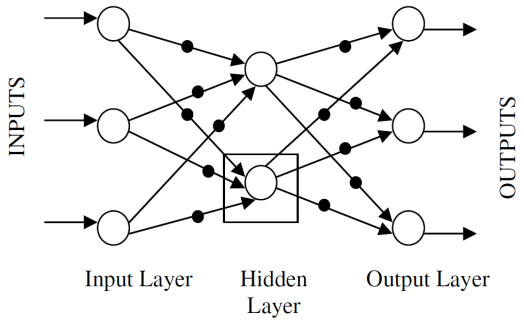

Fig. 1 Basic structure of ANN [39]

In order to teach the neural network, sufficient amount of data is needed. The data can either be provided by experiments or by simulations, including finite element method [39]. A large enough number of FEM simulations was also performed in here-presented study with a goal to provide data points on which the neural network is trained. One of the advantages of using ANN model is easy construction of said model on provided input and output data values with the goal of accurately predicting process dynamics [42].

Machine learning, deep learning, artificial intelligence and more specifically artificial neural networks are being used in many fields, including state of tools, defect detection, forming processes and material science [43-46]. In the study by Czinege and Harangozo [46], experimental data from tensile tests and Nakazima tests were used as input data for the ANN. The ANN models allowed estimation of points of the forming limit curve [46]. ANN models gave high correlation coefficient between predicted and measured values, which was better compared to capabilities of other linear and non-linear models [46]. Multi-layer perceptron (MLP) artificial neural networks are good for classification and for regression, which is also one of the reasons for being used in the study by Czinege and Harangozo [46]. MLP ANN requires a proper selection of the number of hidden layers and data splitting into training set, test set and validation set [46, 47]. In order to predict the flow curves of ZAM100 magnesium alloy sheets under hot-forming conditions as a function of process parameters, El Mehtedi *et al.* [48] developed an empirical model based on ANNs. ANN model predicted the flow stress as a function of strain, strain rate and temperature [48]. The ANN from the study by El Mehtedi *et al.* [48] had 6 input parameters and one output of equivalent stress, and it also had two hidden layers with 6 neurons each. The back-propagation training and validation of the multi-layer feed forward ANN was performed using MATLAB software [48]. Great capabilities of the set model were proven with excellent fitting between experimental and predicted curves [48]. For the reason of evaluating the prediction capabilities, the correlation coefficient (R) was considered, which compares predicted values and experimentally produced data [48]. The model for predicting flow curves requires a sufficient number of experiments to obtain the necessary data on which it can be trained, which is expensive and time-consuming

[48]. ANN models are often used also in the field of metal forming. In the study by Gondo and Arai [37] an ANN was developed for metal spinning using tool-path parameters, the size of the blank, size of the tools and the height and the thickness of the part. In the study by Xia *et al.* [45] multi-layer feed-forward perceptron ANN models with back-propagation were used to investigate the influence of rolling parameters on the rolling force, rolling power, and slip of tandem cold rolling. Different ANN architectures had been tested and the ANN configuration of one hidden layer with 9 neurons provided the best results [45]. In the study by Kazan *et al.* [39] a prediction model using ANN was developed in the field of wipe-bending. The training of the ANN model was done on the data provided by FEM simulations [39]. In the study by Sivasankaran *et al.* [42] a feed forward back-propagation neural network was presented for predicting and avoiding surface failure, including wrinkling, during pure aluminium sheet drawing through a conical die. The neural network had two hidden layers with different numbers of neurons for different grades of aluminium sheets tasted [42].

The study by Babu *et al.* [49] focused on developing an expert system using ANN to predict the deep drawing behaviour of welded blanks made of steel grade and aluminium alloy. FEM code is used for forming simulation and data generation for ANN training [49]. ANNs with one hidden layer with 6 neurons, 6 neurons on the input layer and one neuron on the output layer are used for four different output parameters, including depth of drawing [49]. In the study by Manoochehri and Kolahan [50] an ANN was developed based on FEM results in the case of deep drawing, where important process parameters as inputs and process characteristics as outputs were considered. FEM models were verified with experimental tests using same parameter values, including stainless steel 304 (AISI 304) with 0.5 mm thickness with its mechanical properties and anisotropic coefficients [50]. In the study by Manoochehri and Kolahan [50] ABAQUS/Explicit software was used to develop FEM models of the deep drawing process, where the depth of drawing was 30 mm. The input parameters considered were blank holder force, punch radius, die radius, friction coefficient between punch and blank as well as die and blank, while the output parameter was minimum sheet thickness after forming [50]. An ANN with two hidden layers was developed in MATLAB software [50].

2. Material and methods

2.1 Used materials

TRIP steels prove highly effective in manufacturing automotive components that undergo significant work hardening during crash deformation and necessitate substantial energy absorption. Additionally, these steels are particularly well-suited for forming intricate and challenging to form parts due to their exceptional formability and hardening characteristics. In the experimental research, a double-sided galvanized steel sheet TRIP RAK40/70 Z100MBO with a thickness of 0.75 mm was utilized. To determine the mechanical properties, a uniaxial tensile test was conducted on the TIRAtest2300 machine (Fig. 2) according to the STN EN ISO 6892-1:2020 standard. During the examination, 5 test samples were assessed in three directions: 0°, 45°, and 90° degrees with respect to the rolling direction (see Fig. 3). The mechanical properties obtained using uniaxial tensile test are displayed in Table 1. The chemical composition of the experimental material TRIP RAK40/70 Z100MBO is shown in Table 2.

Table 1 Mechanical properties of TRIP RAK40/70 Z100MBO

RD (°)	$R_{p0,2}$ (MPa)	R_m (MPa)	A_{80} (%)	r (-)	r_m (-)	Δr (-)	n (-)
0	435	764	29	0.702			0.298
45	443	763	29	0.884	0.834	-0.100	0.294
90	449	764	31	0.867			0.279

Table 2 Chemical composition of TRIP RAK40/70 Z100MBO wt. %

C	Mn	Si	P	S	Al	Nb	Ti	V	Mo	Cr
0.204	1.683	0.199	0.018	-	1.731	0.004	0.009	0.004	0.008	0.055

Fig. 2 TIRAtest2300 testing machine

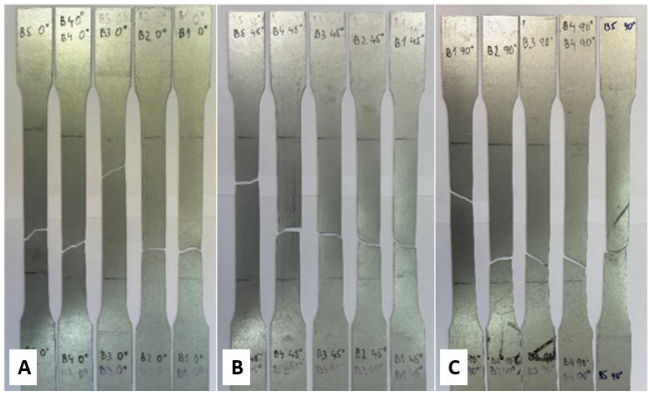

Fig. 3 Samples after uniaxial tensile test: a) in the RD direction 0°; b) in the RD direction 45°; c) in the RD direction 90°

2.2 Deep drawing test

Deep drawing is a sheet metal forming technique where a sheet metal blank is radially drawn into a forming die by mechanical energy. This process is notably influenced by material properties, as well as geometric and technological parameters. Key material parameters include elasticity, plasticity, and anisotropy. Moreover, parameters like punch velocity, blank holding force, and lubrication are crucial, besides the radius of the punch and die, the thickness of the blank, and the clearance between the punch and die. Improperly defining these parameters can lead to defects such as surface scratches, wrinkling, and tearing due to excessive thinning. The paper focuses on analysing how various technological and material parameters affect the key characteristics of the product and its forming process. These characteristics include deep-drawing force, earing, and thinning.

In the experimental research, three circular blanks with a diameter of 95 mm were cut from the sheet metal strip, from which cylindrical cups with a flat bottom were subsequently drawn on an experimental deep drawing tool (Fig. 4a) with the parameters shown in Fig. 4b. In the deep drawing test, oil was used as a lubricant to reduce the coefficient of friction. The holding force was set to 18000 N.

During the deep drawing process, it is essential to comprehend the maximum deep drawing force and the impact of input parameters on its magnitude. This understanding is fundamental for selecting the appropriate machine with the designated force. To measure the force during our experiment, we employed a load cell integrated into the forming press. During the deep drawing test, the load cell recorded and transmitted force data to a connected data acquisition system. The force was monitored and recorded throughout the entire process of deep drawing.

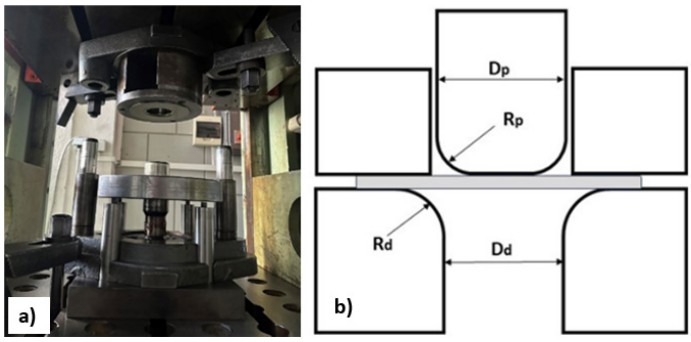

Fig. 4 a) Experimental deep drawing tool, b) parameters of the tool, where: D_p (punch diameter) = 50 mm, D_d (die diameter) = 52.4 mm, R_p (punch radius) = 5 mm, R_d (die radius) = 5.5 mm

Furthermore, we focused on understanding the influence of the parameters on earing, characterized by the development of a wavy edge at the open end of the cup. In this paper, earing was assessed as the difference between the highest (H_{max}) and lowest (H_{min}) measured heights on the cups, as defined by Eq. 1, where ΔH represents ear height.

$$\Delta H = H_{max} - H_{min} \tag{1}$$

According to the value of Δr, it is possible to determine the susceptibility of the sheet to the formation of ears during deep drawing. Ears are formed in the directions of the sheet where the value of the coefficient of normal anisotropy r is maximum, if:

- $\Delta r > 0$ ears will form in the directions of 0° and 90° to the rolling direction,
- $\Delta r = 0$ ears will not form,
- $\Delta r < 0$ ears will form in the direction of 45°.

The height of the ears (Fig. 5a) was measured with a sliding calliper at eight locations on the cups (Fig. 5b). Subsequently, according to Eq. 1, the maximum difference in the height of the cups was calculated.

We also focused on the thinning of the sheet, which was expressed by the t_{min} value, which represented the lowest measured value of the sheet thickness after forming. Thinning of the blank typically occurs at the transition point from the cylindrical part to the bottom of the blank. Excessive thinning in these areas can lead to the formation of cracks. The thinning itself is affected by the initial thickness of the sheet metal and by the diameter of the tool. When assessing the impact of these parameters on thinning, it is crucial not to overlook the material parameters.

After measuring the heights, the experimental cups were cut in half, allowing us to measure the thickness of the cups and obtain the values of thinning across the cross-section. The thinning of the sheet was measured using an optical microscope (Fig. 6a) at the transition point between the cylindrical part and the bottom of the cup as shown in Fig. 6b.

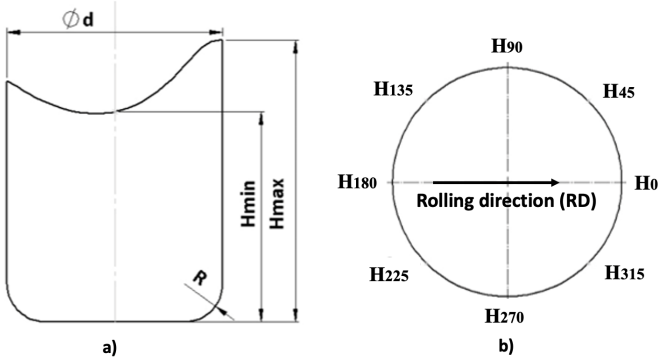

Fig. 5 a) Ear height on the cup, b) Measurement of ear heights on the cup

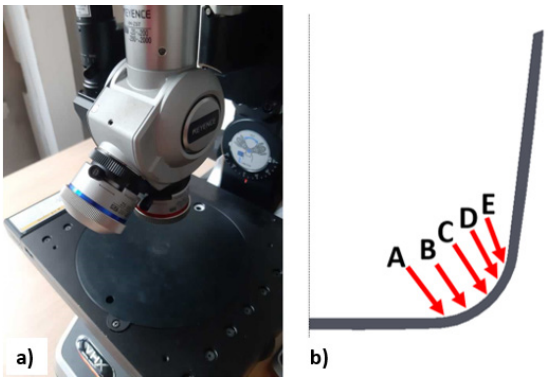

Fig. 6 a) Microscope used for thickness measurement, b) thickness measurement points

2.3 Finite element method setup

The simulation of the deep drawing process was performed using the ABAQUS simulation software environment, utilizing the explicit method. The CAD model of the drawing tool used in the simulation had identical dimensions to the experimental tool (see Fig. 4b). The blank model was given the characteristics of TRIP steel, which were acquired through the uniaxial tensile test (see Table 1). The material density was 7850 kg/m^3, the Young's modulus was 210,000 MPa, and the Poisson ratio was 0.33. During the simulations, the Hollomon approximation was used to describe the flow curve of the material. The sheet material was considered anisotropic using yield criteria according to Hill. The simulation time for the explicit simulation method was set to 0.5 seconds.

According to the finite element method, the simulation of technological processes requires the meshing of the entire set of 3D objects (rigid as well as deformable models) with finite elements. For all rigid bodies (punch, die, and blank holder), R3D4 quadrilateral shell finite elements and R3D3 transition triangle elements were used. In terms of workpiece meshing, concentric mapped quadrilateral finite elements S4R were chosen for the outer section, while a freely meshed combination of quadrilateral finite elements (S4R) and triangular finite elements (S3) was utilized for the central part.

Since the size of the blank was one of the parameters that was regularly changed in each simulation, the number of elements was different in each simulation. Table 3 shows the number and types of elements used in simulations for every 3D model used in simulations. Fig. 7 shows the mesh of the blank used in the simulation.

Table 3 Number and types of elements used in simulations

Object	Number of elements	Type of element
Punch	1634	R3D4, R3D3
Die	4200	R3D4
Blank Holder	2040	R3D4, R3D3
Blank	varied	S4R, S3

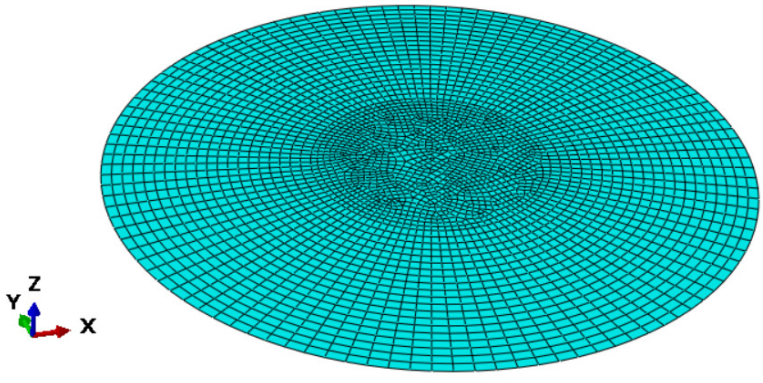

Fig. 7 Mesh of blank CAD model

The procedure involved conducting 50 simulations in which 8 independent input parameters were randomly varied. These parameters include blank diameter (D_0), blank holding force (F_{bh}), friction coefficient (f), material constant (C), hardening exponent (n), and normal anisotropy coefficient values (r) in the 0°, 45°, and 90° directions. Additionally, one dependent parameter, the yield strength (R_p). Table 4 displays the range of input parameters within which values were randomly selected for individual simulations. Values from these intervals were selected randomly for each simulation using the random function in Microsoft Excel. Table 5 shows the values of the input parameters used in the simulations.

Table 4 Range of input parameters used in simulations

Parameter	Minimal value	Maximal value
D_0 (mm)	86	102
F_{bh} (N)	16000	20000
f (-)	0.05	0.20
Rp (MPa)	300	700
C (MPa)	900	1800
n (-)	0.2	0.35
r_0 (-)	0.6	1
r_{45} (-)	0.6	1
r_{90} (-)	0.6	1

Table 5 Randomly selected input values used in individual simulations

Simulation number	D_0 (mm)	F_{bh} (N)	f (-)	R_p (MPa)	C (MPa)	n (-)	r_0 (-)	r_{45} (-)	r_{90} (-)
1	88.4	17778	0.11	491	1512	0.23	0.93	0.74	0.89
2	96.9	18078	0.15	308	1038	0.28	0.64	0.8	0.65
3	100.4	19788	0.07	418	1372	0.27	0.63	0.62	0.75
4	90.6	18082	0.19	308	1112	0.3	0.99	0.7	0.72
.....	...	...	...	...	...	...	...	...	...
50	87.8	16560	0.1	385	1076	0.23	0.92	0.69	0.95

2.4 Artificial neural network

With the aim of making predictions of forming force value, sheet metal thinning and ear height for the deep drawing process and product, artificial neural networks (ANNs) had been set up. For this study, a separate ANN was set up for every output parameter that considered all 9 input parameters. In order to allow faster training of the neural network and good regression of the results, multilayer perceptron artificial neural networks (MLP ANN) had been used. This is an ANN model that used backpropagation learning algorithm. The basis of MLP ANN remains the same, meaning transformation of input values into output values or predictions. To better understand the process of MLP ANN, Eq. 2 shows the basic function, where y is the output value, x is the input value, w are weights and b are biases.

$$y = f(net) = f\left(\sum_{i=1}^{n} w_i x + b\right) \tag{2}$$

The basis for training an ANN is a sufficient number of data points, which was in our case provided by 50 finite element method simulations with different values of input parameter values and their corresponding values of output parameters of forming force, minimum sheet thickness and ear height. To set up the architecture for all three ANNs of three different output parameters, data had to be divided into subsets for training and for testing. A preliminary investigation showed that the best possible division of the data is 90 % for training and the rest for testing, meaning 45 points are used for training and five points out of 50 are used for testing.

Once the lengthy process of training is complete, the set ANNs can be used for prediction purposes. All three ANNs of three considered output parameters are based on the feed-forward multilayer perceptron (MLP) and are thus divided into layers. On every layer there is at least one neuron. The layers present within an MLP ANN are the input, output and at least one hidden layer. On the input layer there are as many neurons as there are input parameters, which in the case of

our study is equal to 9. In the case of our study there is only one neuron on the output layer of all three neural networks which corresponds to one output parameter of either forming force value, minimum sheet thickness or ear height. Within the preliminary study the number of hidden layers was set to five for every neural network and their corresponding output parameter. The same is true for the number of neurons on these five hidden layers, where 60 neurons had been chosen for all five hidden layers for all three neural networks. The configuration of hidden layers and corresponding number of neurons can be written as (60, 60, 60, 60, 60).

Within the neural network the value leaving a specific neuron is affected by the weight and the bias value before entering a specific neuron of the next layer. An important role is played by the activation function which removes certain values and maps modified remaining values. Many different activation functions had been tested in a preliminary study and a decision had been made to use sigmoid or logistic activation function on the neurons of the hidden layers and linear or identity activation function to be used on the output layer of all three set ANNs within this study. Eq. 3 represents sigmoid and Eq. 4 the linear activation function. Additionally, Adaptive Moment Estimation (ADAM) solver type had been used in MATLAB program environment, used for training of the ANNs and for predictions made used trained ANNs. Initial learning rate value was chosen to be 0.1 for all set ANNs and the value of the learning rate remained constant throughout the neural network training process. L2 regularisation was used, and its value chosen as 0.001 for all ANNs within the study. The essential hyperparameter values for all three ANNs are written in Table 6. For a better understanding of the ANN configurations for this study, Fig. 8 shows a schematic presentation of all the neurons within input, output and hidden layers. With all the chosen values of hyperparameters that define the ANN architecture, the training of three different ANNs of all three tested output parameters has been carried out.

$$f(x) = \frac{1}{1 + e^{-x}} \tag{3}$$

$$f(x) = x \tag{4}$$

Table 6 Hyperparameters chosen for three ANNs within the study for the corresponding output parameters of forming force, minimum sheet thickness and ear height

Hidden layer sizes	Activation function	Solver	Initial learning rate	Learning rate type	L2
(60 60 60 60 60)	Sigmoid	ADAM	0.100	Constant	0.001

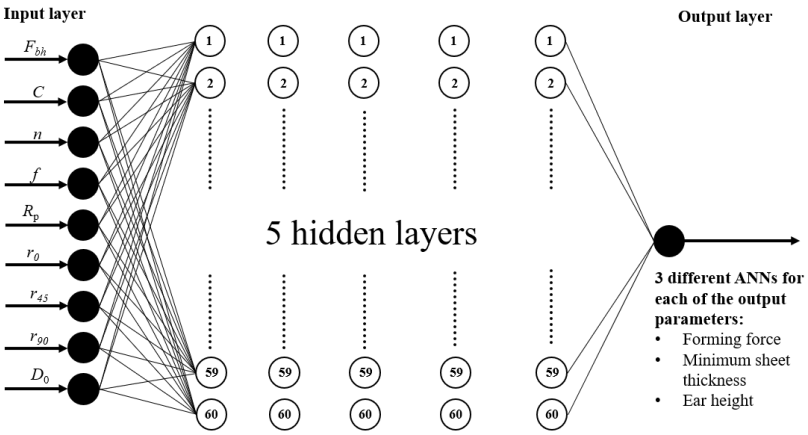

Fig. 8 Schematic representation of the ANNs used within here presented study; input layer with 9 neurons of the 9 tested input parameters, 5 hidden layers with 60 neurons each and an output layer with one neuron for one output parameter within a single ANN.

3. Results and discussion

As part of the deep drawing test, three cups with a flat bottom were drawn out of circular blanks with a diameter of 95 mm. Three parameters were examined: deep drawing force, minimal thickness, and ear height. Fig. 9 shows cups from TRIP RAK40/70.

Fig. 9 Cups made of TRIP RAK40/70 steel after deep drawing test

Within the framework of the experiment deep drawing forces with values of 84315 N for cup 1, 84490 N for cup 2 and 84490 N for cup 3 were measured. These values were measured by subtracting the holding force from the maximum force measured. The plot of the forces is shown in Fig. 10.

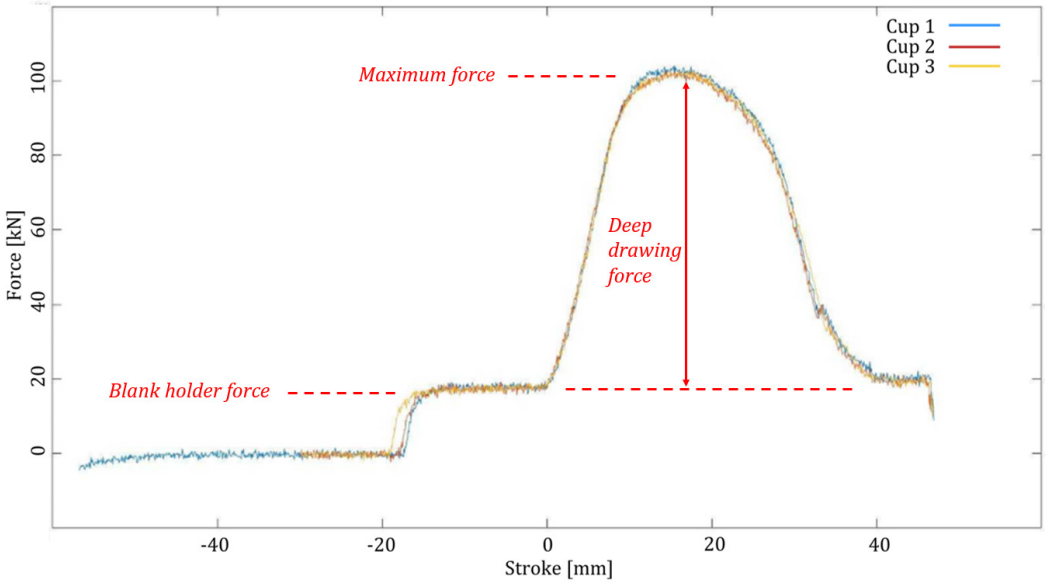

Fig. 10 The course of measured force during the experiment of deep drawing

The measured values of the ear heights in the eight measured directions are shown in Table 7. The ΔH value (the difference between the maximum and minimum ear height) was calculated for each cup, and the average value was subsequently determined.

As shown in Table 7, the most significant disparity in the measured heights occurred at cup 3, where the discrepancy between the maximum and minimum height reached 1.31 mm. The arithmetic average for the parameter ΔH was calculated to be 1.23 mm.

The sheet thickness after the deep drawing test was measured at five points along the cross-section of the cups at the transition from the cylindrical part to the bottom of the cups. The examined sheet thicknesses after the deep drawing tests are shown in Table 8. From the measured thicknesses, the smallest obtained value (t_{min}) was evaluated. From the value $t_{min,}$ the arithmetic average was calculated within the three cups. Fig. 11 shows the measurement of sheet metal thickness at the bottom radius of the second cup.

Table 7 Ear height values of the cups in eight directions along with the calculated ΔH value

Cup number	H_0 (mm)	H_{45} (mm)	H_{90} (mm)	H_{135} (mm)	H_{180} (mm)	H_{225} (mm)	H_{270} (mm)	H_{315} (mm)	ΔH (mm)
1	33.61	34.11	33.07	33.17	32.93	33.25	32.86	33.84	1.25
2	32.95	33.96	33.58	34.09	33.22	33.58	32.98	33.65	1.14
3	33.65	34.52	33.67	34.02	33.53	33.95	34.02	34.84	1.31
								avg. ΔH (mm)	1.23

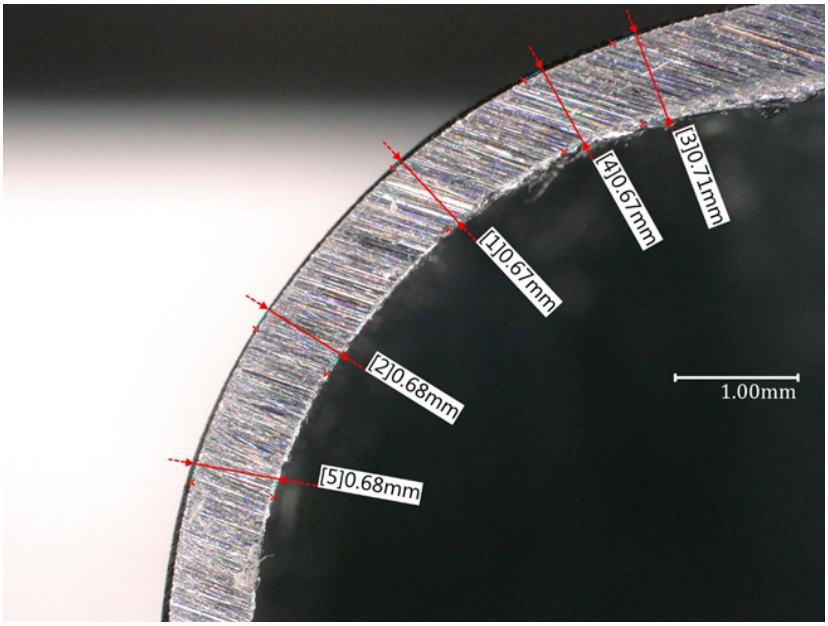

Fig. 11 Measurement of thinning at the bottom radius of the test cup

Table 8 Minimal thickness values of the cups in five measured points along with the t_{min} value

Cup number	t_A (mm)	t_B (mm)	t_C (mm)	t_D (mm)	t_E (mm)	t_{min} (mm)
1	0.65	0.64	0.64	0.64	0.67	0.64
2	0.71	0.67	0.67	0.68	0.68	0.67
3	0.65	0.62	0.62	0.62	0.65	0.62
					avg. t_{min} (mm)	0.64

A deep drawing test simulation was performed with same parameter values as the performed experiments. The explicit method in the ABAQUS simulation program was used. The maximum deep drawing force, thinning value, and ear heights were measured in eight directions, from which the ΔH value was calculated using Eq. 1. Fig. 12 shows the cup shape after the performed simulation.

The results of the 50 simulations present the influence of 9 input parameters on the three monitored outputs, which are the maximum deep drawing force, minimum sheet thickness and earing. The results of 50 simulations in which the input parameters were randomly selected (see Table 5) from the interval of values (see Table 4) are shown in Table 9. As we can see, changing the 9 input parameters monitored significantly affects the observed output parameters.

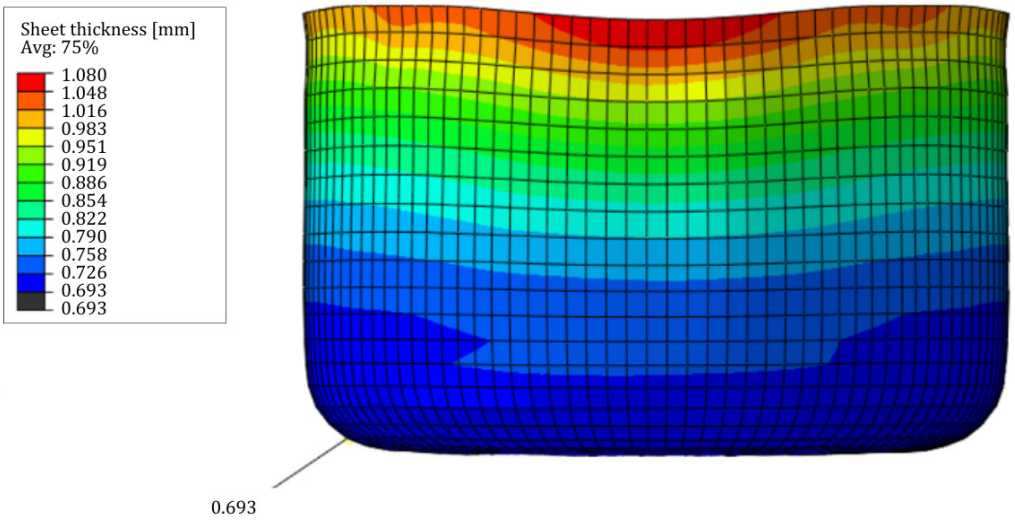

Fig. 12 Result of the simulation of deep drawing test using ABAQUS

Table 9 Results of 50 simulations carried out in ABAQUS simulation software

Simulation number	F_{max} (N)	t_{min} (mm)	H_{max} (mm)	H_{min} (mm)	ΔH (mm)
1	77814	0.713	27.32	26.41	0.91
2	63907	0.641	35.26	33.92	1.34
3	84826	0.653	37.11	36.52	0.59
4	62045	0.672	30.01	28.79	1.22
.....	...	...	...	...	...
50	54482	0.713	26.34	25.07	1.27

With all the chosen values of hyperparameters that define the ANN architecture, the training of three different ANNs of all three tested output parameters has been carried out. Trained neural networks allow for predictions to be carried out. Figs. 13, 14 and 15 show diagrams comparing original output values provided by simulations and predicted values using trained ANNs that were provided by using the same input parameter values. If the predictions perfectly matched the original values, then a straight line would be seen on the diagrams. But as we can see, a slight discrepancy is evident. To further understand the predictive capabilities of all three ANNs two coefficients were calculated, namely correlation coefficient R and coefficient of determination R^2. Using the MATLAB program environment, the value for R squared was calculated automatically at the end of the ANN training process. R^2 value (Table 10) was calculated with the use of Eq. 5, where simulation output parameter values y_i are compared to ANN predicted values $\hat{y}_i$. For the predicted values using ANN, same input parameter values were used as in the case of the FEM simulations. To better understand the predictive capabilities of ANNs and to show the general correctness of the simulations performed, Fig. 16, Fig. 17 and Fig. 18 show a comparison of the values obtained with an experimental method, an explicit simulation and a neural network using the same input parameters (see Table 11).

Table 10 Evaluation of set ANNs for three different output parameters using R and R^2

Output parameter	R	R^2
Forming force	0.975	0.949
Sheet metal thickness	0.953	0.907
Ear height	0.926	0.844

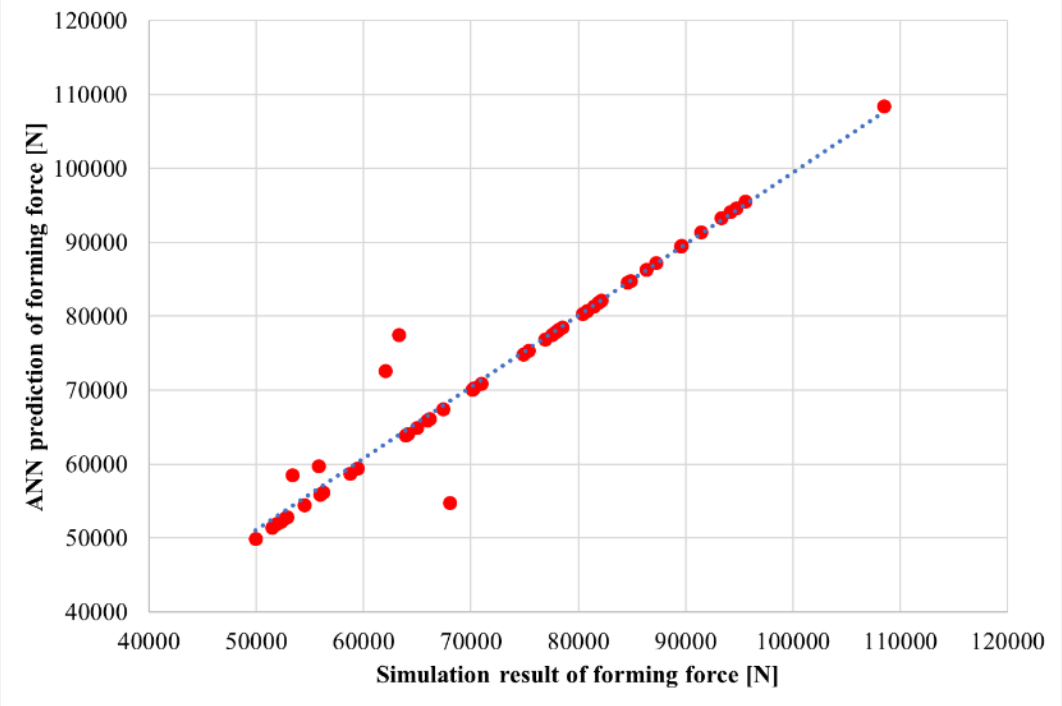

Fig. 13 Comparison of simulation results and predicted values by ANN for the output parameter of forming force value

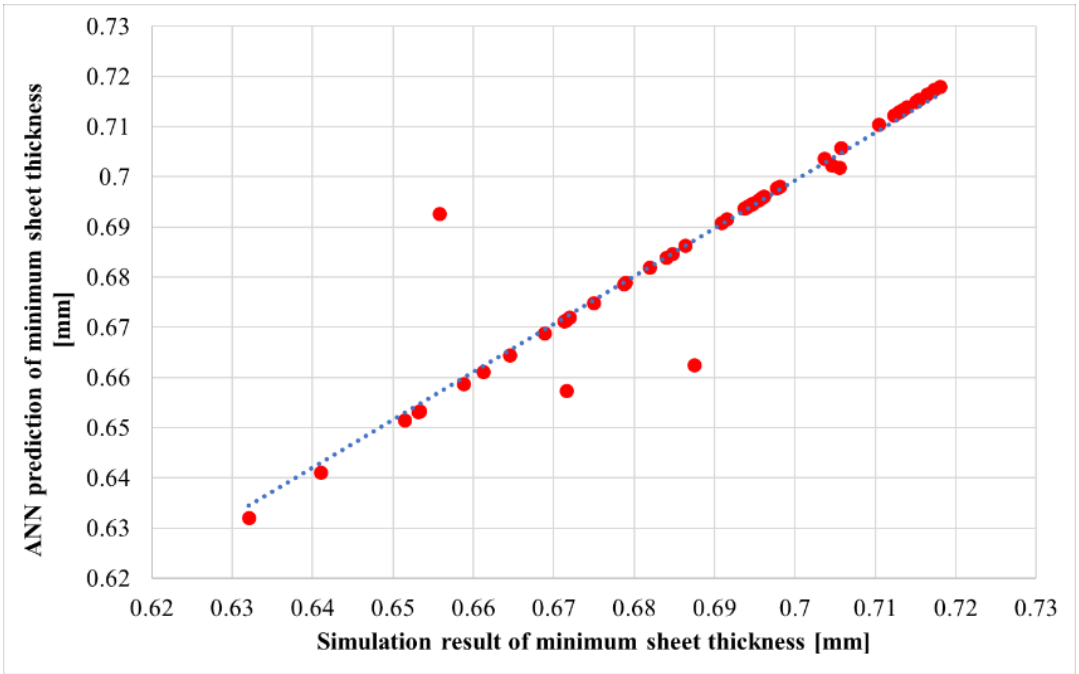

Fig. 14 Comparison of simulation results and predicted values by ANN for the output parameter of minimum sheet thickness

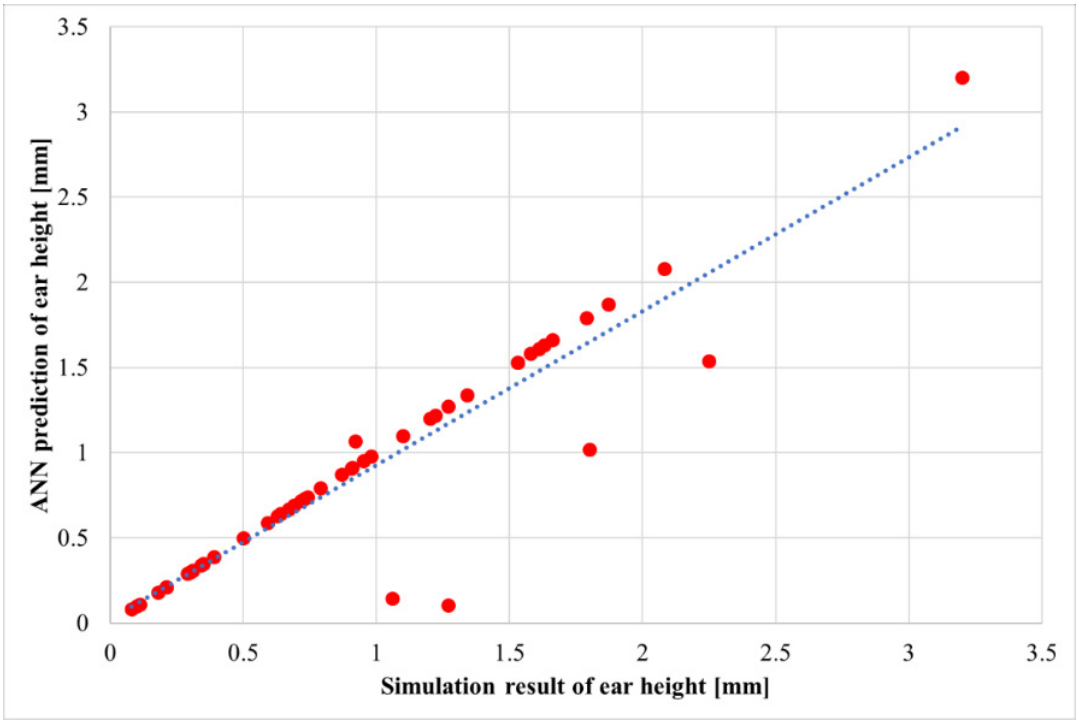

Fig. 15 Comparison of simulation results and predicted values by ANN for the output parameter of ear height

Table 11 Parameters used in the experiment, explicit simulation and ANN with results shown in Figs. 16 to 18

D_0 (mm)	F_{bh} (N)	f (-)	R_p (MPa)	C (MPa)	n (-)	r_0 (-)	r_{45} (-)	r_{90} (-)
95	18000	0.1	422.3	1488	0.28	0.702	0.884	0.867

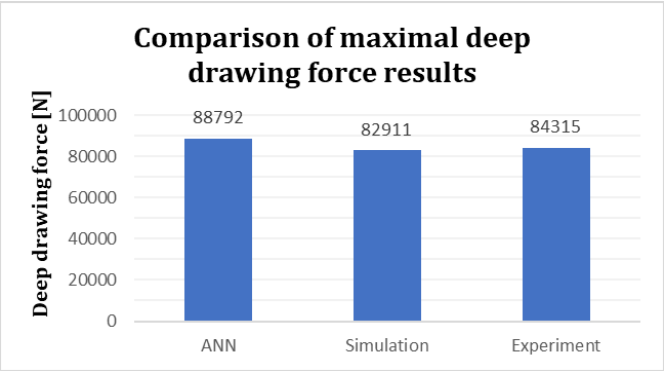

Fig. 16 Comparison of measured and calculated maximal deep drawing force values

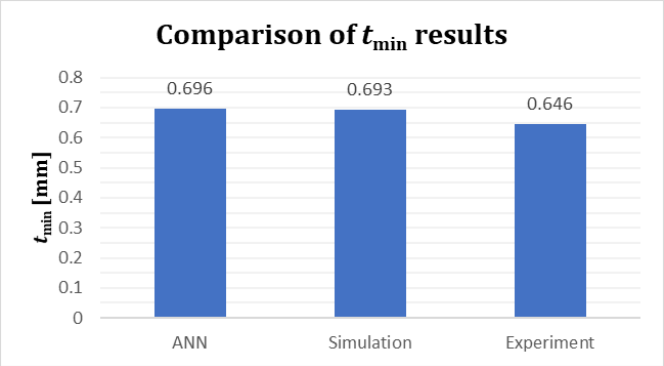

Fig. 17 Comparison of measured and calculated t_{min} values

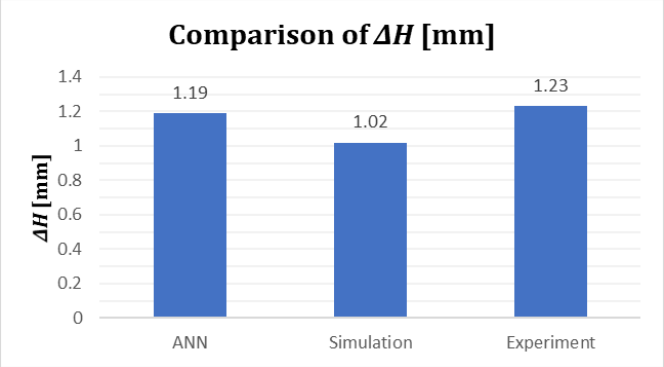

Fig. 18 Comparison of measured and calculated ΔH values

4. Conclusion

Optimisation of the deep drawing process is crucial due to its wide application in the automotive industry. Constantly increasing requirements for reducing emissions force designers to utilize high-strength materials, resulting in a reduction in the weight of structures. The demands on the industry are constantly growing, leading to the development of new methods for optimizing the deep drawing process. Artificial intelligence plays a pivotal role in this, with its increasingly frequent integration into technological processes. Thanks to constant improvement in this field, the output parameters of deep drawing can be predicted. In this study, ANN was used to predict the output parameters, the results of which were compared with experimental values and simulation using the explicit integration method.

The paper has focused on the analysis of various technological and material parameters that influence the key properties of the forming process. The results of the experiment demonstrate the potential for employing various methods and their integration to predict selected output parameters, such as evaluating the maximum deep drawing force, thinning and earing expressed

through the difference between the maximum and minimum yield height. In the experimental part of the research, a deep-drawing tool with defined geometry was used. Double-sided galvanized steel sheet TRIP RAK40/70 was chosen as the test material. TRIP steels represent a material that combines exceptional forming properties with strength.

In the simulations, eight independent input parameters and one dependent input parameter, which was the yield strength (R_p), were randomly varied. Independent input parameters include blank diameter (D_0), blank holding force (F_{bh}), coefficient of friction (f), material constant (C), strain hardening exponent (n) and normal anisotropy coefficient values (r) at 0°, 45°, and 90° directions. The experiment proved the correctness of the simulation of the deep drawing process for the prediction of the selected output parameters, considering the variability of the use of possible input parameters that affect the forming process. In order to predict the selected output parameters, artificial neural networks were developed. Each output parameter was modeled by its own dedicated ANN, considering all nine input parameters for this study. In order to provide a sufficient amount of data to train the ANNs, a sufficient number of simulations had to be carried out. Running a simulation took between one to two hours, which is a lengthy process. The training of the ANNs and the predictions with the trained ANNs were performed on a computer with an Intel Core i7-1065G7 processor with 3.6 GHz and 16 GB RAM. The training of the ANNs took several minutes, while the prediction process took less than one second after the input values of all input parameters were provided to the ANN.

As can be seen from Table 10, the prediction of the maximum deep drawing force using ANN achieved the best results within all evaluated parameters with a value of $R^2 = 0.949$. When entering the input parameters, which were identical to the performed experiment, the prediction using ANN reached the maximum deep drawing force of 88792 N. During the simulation, it was measured as 82911 N compared to the deep drawing force of 84315 N during the experiment. The same values of the input parameters used in the experiment and in the simulation and provided to the ANN are listed in Table 11.

One of the main difficulties in the deep drawing process lies in optimizing the thinning as it can lead to reduced mechanical strength in the final product. If the thinning reaches a critical value, it can lead to failure. As part of the experiments, thinning was evaluated on three cups. The measured minimal thickness (t_{min}) reached the value of 0.64 mm for cup 1, 0.67 mm for cup 2 and 0.62 for cup 3. When comparing the arithmetic mean of these three values, we register a difference of 0.047 mm compared to the results from the simulation using the explicit method. In all three experimental cups, a smaller wall thickness value was measured compared to the simulation, where t_{min} reached a value of 0.693 mm using same input parameter values listed in Table 11. When comparing original output values provided by 50 simulations and predicted values using trained ANNs that were provided same 50 sets of input parameter values, R^2 of 0.907 was calculated. The trained ANN predicted a minimum thickness of 0.696 mm when entering exact values of the experiment listed in Table 11. The most significant discrepancy in predicting the output parameters was measured in the case of ear height, evaluated using the ΔH parameter. When comparing the difference in maximum and minimum cup height, the deviation between simulation and experimental results was found to be 0.21 mm for the same input parameter values. ANN showed superior performance in this regard, with the difference narrowing to 0.04 mm. The calculated R^2 value for the ANN was 0.844 when comparing 50 results from simulations and predictions made with trained ANN using same input parameter values. With this value of R^2 parameter, we can state that this value was influenced by the manual measurement of heights after the experiments and simulations, that were utilized to train the ANN.

The conducted research provides a strong foundation for the continued utilization of the Finite Element Method and Artificial Neural Network techniques in the field of predicting the critical output parameters of deep drawing such as maximal deep drawing force, thinning and earing. With the aim of predicting the crucial output parameter values of the deep drawing process and providing additional control of the process itself, our future work will focus on the following:

- Analysis of different tool geometry for the production of a cylindrical cup with a smaller inner diameter. Experiments, simulations and ANNs will be set for the use of a smaller tool and compared with the results obtained with the tool in the study presented here.
- Analysis of different steel grades and their performance during the deep drawing process. Further extension of the predictive capabilities of ANN models for more extensive material parameter ranges.
- Analysis of deep drawing of more complex part shapes. Experiments and simulations for different tool and thus part shapes would enable the development of more flexible ANN models that would allow the prediction of important deep drawing output parameters for a larger number of selected part shapes.

Acknowledgement

This paper was written with the financial support of the granting agency APVV within the project solution APVV-21-0418 and support from the Slovenian Research Agency ARIS (research core funding No. P2-0248).

References:

[1] Spišák, E., Majerníková, J. (2014). A study of thickness change of spherical cup made from TRIP steel after hydraulic bulge test, *Key Engineering Materials*, Vol. 635, 157-160, doi: 10.4028/www.scientific.net/KEM.635.157.
[2] Lai, M., Brun, R. (2007). Latest developments in sheet metal forming technology and materials for automotive application: The use of ultra-high strength steels at fiat to reach weight reduction at sustainable costs, *Key Engineering Materials,* Vol. 344, 1-8, doi: 10.4028/www.scientific.net/KEM.344.1.
[3] Bright, G.W., Kennedy, J.I., Robinson, F., Evans, M., Whittaker, M.T., Sullivan, J., Gao, Y. (2011). Variability in the mechanical properties and processing conditions of a High Strength Low Alloy steel, *Procedia Engineering,* Vol. 10, 106-111, doi: 10.1016/j.proeng.2011.04.020.
[4] Thomas, S.K., Ali, A., AlArjani, A., Attia, E.-A. (2022). Simulation based performance improvement: A case study on automotive industries, *International Journal of Simulation Modelling*, Vol. 21, No. 3, 405-416, doi: 10.2507/IJSIMM21-3-606.
[5] Visagan, A., Ganesh, P. (2022). Parametric optimization of two point incremental forming using GRA and TOPSIS, *International Journal of Simulation Modelling*, Vol. 21, No. 4, 615-626, doi: 10.2507/IJSIMM21-4-622.
[6] Spišák, E., Majerníková, J. (2013). Analysis of variance of mechanical properties of sheets as the input parameters for simulation of processes, *Acta Metallurgica Slovaca,* Vol. 18, No. 2-3, 109-116.
[7] Dykeman, J., Hoydick, D., Link, T., Mitsuji, H. (2009). Material property and formability characterization of various types of high strength dual phase steel, *SAE Technical Paper 2009-01-0794,* SAE International, doi: 10.4271/2009-01-0794.
[8] Takahashi, M. (2003). Development of high strength steels for automobiles, *Nippon Steel Technical Report*, No. 88, 2-7, from *https://www.nipponsteel.com/en/tech/report/nsc/pdf/n8802.pdf*, accessed February 7, 2024.
[9] Bleck, W., Brühl, S., Gerdemann, F.L.H., Prahl, U. (2007). Gefüge-Engineering bei kaltumformbaren Stählen*, Umformtechnik: Stahl und NE-Werkstoffe; der Zukunft Form geben; Tagungsband / 22. ASK, Aachener Stahlkolloquium*, 08/09. März 2007, Eurogress Aachen. Institut für Bildsame Formgebung; Institut für Eisenhüttenkunde, RWTH, Rheinisch-Westfälische Technische Hochschule Aachen, 267-280.
[10] Heinemann, G. (2004). *Virtuelle Bestimmung des Verfestigungsverhaltens von Bändern und Blechen durch verformungsinduzierte Martensitbildung bei metastabilen rostfreien austenitischen Stählen,* Dissertation, Eidgenössische Technische Hochschule Zürich.
[11] Behrens, B.-A., Hübner, S., Voges-Schwieger, K., Weilandt, K. (2007). Verformungsinduzierte Martensitevolution zur lokalen Festigkeitssteigerung, *UTF Science* II, 1-4.
[12] Papaefthymiou, S. (2005). Failure mechanisms of multiphase steels, Dissertation, RWTH Aachen, Aachen, Shaker Verlag.
[13] Stefanovska, E., Pepelnjak, T. (2022). Development of a flexible tooling system for sheet metal bending, *Advances in Production Engineering & Management*, Vol. 17, No. 3, 311-325, doi: 10.14743/apem2022.3.438.
[14] Spišák, E., Greškovič, F., Maňková, I., Brezinová, J., Kráľ, J., Slota, J., Draganovská, D., Viňaš, J., Kaščák, Ľ. (2011). *Strojárske technológie*, Strojnícka fakulta TU v Košiciach, Košice, Slovakia.
[15] Dwivedi, R., Agnihotri, G. (2017). Study of deep drawing process parameters, *Materials Today: Proceedings.* Vol. 4, No. 2, Part A, 820-826, doi: 10.1016/j.matpr.2017.01091.
[16] Semiatin, S.L. (2006). Introduction to sheet-forming processes, In: Semiatin (ed.), *Metalworking: Sheet Forming* Vol. 14B, ASM International, Almere, Netherlands, 319-333, doi: 10.31399/asm.hb.v14b.9781627081863.
[17] Spišák, E., Slota, J., Majerníková, J., Kaščák, Ľ., Malega, P. (2012). Inhomogeneous plastic deformation of tinplates under uniaxial stress state, *Chemické listy.* Vol. 106, 537-540.
[18] Joshi, A.R., Kothari, K.D., Jhala, R.L. (2013). Effects of different parameters on deep drawing process: Review, *International Journal of Engineering Research & Technolog.* Vol. 2, No. 3.

[19] Benke, M., Schweitzer, B., Hlavacs, A., Mertinger, V. (2020). Prediction of earing of cross-rolled al sheets from {h00} pole figures, *Metals,* Vol. 10, No. 2, Article No. 192, doi: 10.3390/met10020192.
[20] Hlavacs, A., Szucs, M., Mertinger, V., Benke, M. (2021). Prediction of earing of hot-rolled al sheets from pole figures, *Metals*, Vol. 11, No. 1, Article No. 99, doi: 10.3390/met11010099.
[21] Dong, W., Wang, Q., Wang, X., Wang, B. (2018). Stress analysis of cylindrical parts during deep drawing based on Dynaform, *IOP Conference Series Materials Science Engineering*, Vol. 423, Article No. 012166, doi: 10.1088/1757-899X/423/1/012166.
[22] Colgan, M., Monaghan, J. (2003). Deep drawing process: Analysis and experiment, *Journal of Materials Processing Technology*, Vol. 132, No. 1-3, 35-41, doi: 10.1016/S0924-0136(02)00253-4.
[23] Seth, M., Vohnout, V.J., Daehn, G.S. (2005). Formability of steel sheet in high velocity impact, *Journal of Materials Processing Technology,* Vol. 168, No. 3, 390-400, doi: 10.1016/j.jmatprotec.2004.08.032.
[24] Huang, Y.-M., Tsai, Y.-W., Li, C.-L. (2008). Analysis of forming limits in metal forming processes, *Journal of Materials Processing Technology,* Vol. 201, No. 1-3, 385-389, doi: 10.1016/j.jmatprotec.2007.11.279.
[25] Chalal, H., Abed-Meraim, F. (2017). Determination of forming limit diagrams based on ductile damage models and necking criteria, *Latin American Journal of Solids and Structures*, Vol. 14, No. 10, 1872-1892, doi: 10.1590/1679-78253481.
[26] Gusel, L., Boskovic, V., Domitner, J., Ficko, M., Brezocnik, M. (2018). Genetic programming method for modelling of cup height in deep drawing process, *Advances in Production Engineering & Management*, Vol. 13, No. 3, 358-365, doi: 10.14743/apem2018.3.296.
[27] Sevšek, L., Baressi Šegota, S., Car, Z., Pepelnjak, T. (2023). Determining the influence and correlation for parameters of flexible forming using the random forest method, *Applied Soft Computing*, Vol. 144, Article No. 110497, doi: 10.1016/j.asoc.2023.110497.
[28] Cwiekala, T., Brosius, A., Tekkaya, A.E. (2011). Accurate deep drawing simulation by combining analytical approaches, *International Journal of Mechanical Sciences*, Vol. 53, No. 5, 374-386, doi: 10.1016/j.ijmecsci.2011.02.007.
[29] Milutinovic, M., Lendjel, R., Baloš, S., Labus Zlatanovic, D., Sevšek, L., Pepelnjak, T. (2021). Characterisation of geometrical and physical properties of a stainless steel denture framework manufactured by single-point incremental forming, *Journal of Materials Research and Technology*, Vol. 10, 605-623, doi: 10.1016/j.jmrt.2020.12.014.
[30] Vrh, M., Halilovič, M., Starman, B., Štok, B., Comsa, D.-S., Banabic, D. (2014). Capability of the BBC2008 yield criterion in predicting the earing profile in cup deep drawing simulations, *European Journal of Mechanics, A/Solids*, Vol. 45, 59-74, doi: 10.1016/j.euromechsol.2013.11.013.
[31] Bandyopadhyay, K., Panda, S.K., Saha, P., Padmanabham, G. (2015). Limiting drawing ratio and deep drawing behavior of dual phase steel tailor welded blanks: FE simulation and experimental validation, *Journal of Materials Processing Technology*, Vol. 217, No. 48-64, doi: 10.1016/j.jmatprotec.2014.10.022.
[32] Dwivedi, R., Agnihotri, G. (2015). Numerical simulation of aluminum and brass material cups in deep drawing process, *Materials Today: Proceedings*, Vol. 2, No. 4-5, 1942-1950, doi: 10.1016/j.matpr.2015.07.159.
[33] Walde, T., Riedel, H. (2007). Simulation of earing during deep drawing of magnesium alloy AZ31, *Acta Materialia*, Vol. 55, No. 3, 867-874, doi: 10.1016/j.actamat.2006.09.007.
[34] Engler, O., Aretz, H. (2021). A virtual materials testing approach to calibrate anisotropic yield functions for the simulation of earing during deep drawing of aluminium alloy sheet, *Materials Science and Engineering: A*, Vol. 818, Article No. 141389, doi: 10.1016/j.msea.2021.141389.
[35] Luyen, T.-T., Tong, V.-C., Nguyen, D.-T. (2022). A simulation and experimental study on the deep drawing process of SPCC sheet using the graphical method, *Alexandria Engineering Journal*, Vol. 61, No. 3, 2472-2483, doi: 10.1016/j.aej.2021.07.009.
[36] Jayahari, L., Balunaik, B., Gupta, A.K., Singh, S.K. (2015). Finite element simulation studies of AISI 304 for deep drawing at various temperatures, *Materials Today: Proceedings*, Vol. 2, No. 4-5, 1978-1986, doi: 10.1016/j.matpr.2015.07.166.
[37] Gondo, S., Arai, H. (2022). Data-driven metal spinning using neural network for obtaining desired dimensions of formed cup, *CIRP Annals*, Vol. 71, No. 1, 229-232, doi: 10.1016/j.cirp.2022.04.044.
[38] Tian, S., Zhang, Z., Xie, X., Yu, C. (2022). A new approach for quality prediction and control of multistage production and manufacturing process based on Big Data analysis and Neural Networks, *Advances in Production Engineering & Management*, Vol. 17, No. 3, 326-338, doi: 10.14743/apem2022.3.439.
[39] Kazan, R., Firat, M., Tiryaki, A.E. (2009). Prediction of springback in wipe-bending process of sheet metal using neural network, *Materials &Design*, Vol. 30, No. 2, 418-423, doi: 10.1016/j.matdes.2008.05.033.
[40] Afshari, D., Ghaffari, A., Barsum, Z. (2022). Optimization in the resistant spot-welding process of AZ61 magnesium alloy, *Strojniski Vestnik/Journal of Mechanical Engineering*, Vol. 68, No. 7-8, 485-492, doi: 10.5545/sv-jme.2022.174.
[41] Berus, L, Klancnik, S, Brezocnik, M, Ficko, M. (2019) Classifying parkinson's disease based on acoustic measures using artificial neural networks, *Sensors,* Vol. 19, No. 1, Article No. 16, doi: 10.3390/s19010016.
[42] Sivasankaran, S., Narayanasamy, R., Jeyapaul, R., Loganathan, C. (2009). Modelling of wrinkling in deep drawing of different grades of annealed commercially pure aluminium sheets when drawn through a conical die using artificial neural network, *Materials & Design*, Vol. 30, No. 8, 3193-3205, doi: 10.1016/j.matdes.2009.01.020.
[43] Spaić, O., Krivokapić, Z., Kramar, D. (2020). Development of family of artificial neural networks for the prediction of cutting tool condition, *Advances in Production Engineering & Management*, Vol. 15, No. 2, 164-178, doi: 10.14743/APEM2020.2.356.

[44] Nguyen, T.P.Q., Yang, C.L., Le, M.D., Nguyen, T.T., Luu, M.T. (2023). Enhancing automated defect detection through sequential clustering and classification: An industrial case study using the Sine-Cosine Algorithm, Possibilistic Fuzzy c-means, and Artificial Neural Network, *Advances in Production Engineering & Management*, Vol. 18, No. 2, 237-249, doi: 10.14743/apem2023.2.470.
[45] Xia, J.S., Khaje Khabaz, M., Patra, I., Khalid, I., Alvarez, J.R.N., Rahmanian, A., Eftekhari, S.A., Toghraie, D. (2023). Using feed-forward perceptron Artificial Neural Network (ANN) model to determine the rolling force, power and slip of the tandem cold rolling, *ISA Transactions*, Vol. 132, 353-363, doi: 10.1016/j.isatra.2022.06.009.
[46] Czinege, I., Harangozó, D. (2024). Application of artificial neural networks for characterisation of formability properties of sheet metals, *International Journal of Lightweight Materials and Manufacture*, Vol. 7, No. 1, 37-44, doi: 10.1016/j.ijlmm.2023.08.003.
[47] Savkovic, B., Kovac, P., Rodic, D., Strbac, B., Klancnik, S. (2020). Comparison of artificial neural network, fuzzy logic and genetic algorithm for cutting temperature and surface roughness prediction during the face milling process, *Advances in Production Engineering & Management*, Vol. 15, No. 2, 137-150, doi: 10.14743/APEM2020.2.354.
[48] El Mehtedi, M., Forcellese, A., Greco, L., Pieralisi, M., Simoncini, M. (2019). Flow curve prediction of ZAM100 magnesium alloy sheets using artificial neural network-based models, *Procedia CIRP*, Vol. 79, No. 661-666, doi: 10.1016/j.procir.2019.02.050.
[49] Babu, K.V., Ganesh Narayanan, R., Saravana Kumar, G. (2010). An expert system for predicting the deep drawing behavior of tailor welded blanks, *Expert Systems with Applications*, Vol. 37, No. 12, 7802-7812, doi: 10.1016/j.eswa.2010.04.059.
[50] Manoochehri, M., Kolahan, F. (2014). Integration of artificial neural network and simulated annealing algorithm to optimize deep drawing process, *The International Journal of Advanced Manufacturing Technology,* Vol. 73, 241-249, doi: 10.1007/s00170-014-5788-5.